AD-Vol. 31, Space Exploration Science and Technologies Research
ASME 1992

DYNAMIC CHARACTERIZATION, MONITORING AND CONTROL OF ROTATING FLEXIBLE BEAM-MASS STRUCTURES VIA PIEZO-EMBEDDED TECHNIQUES

Steven H.-Y. Lai
Controls and Guidance Group
NASA CORE for Aerospace Research
North Carolina A&T State University
Greensboro, North Carolina

ABSTRACT

A variational principle and a finite element discretization technique were used to derive the dynamic equations for a high speed rotating flexible beam-mass system embedded with piezo-electric materials. The dynamic equation thus obtained allows the development of finite element models which accommodate both of the original structural element and the piezoelectric element. The solutions of finite element models provide system dynamics needed to design a sensing system. The characterization of gyroscopic effect and damping capacity of smart rotating devices are addressed. Several simulation examples are presented to validate the analytical solution.

INTRODUCTION

Structural monitoring and control using smart sensing materials has become of importance in recent years due to the rapid development of large flexible structures and flexible mechanical systems. These materials and structures have their own sensing, actuating, tuning, controlling and computational abilities (Gandhi and Thomas, 1989). Typically, smart materials and structures are distributed-parameter systems operating under a variety of service conditions and having a theoretically infinite number of vibration modes. Current design practice is to model the system with a finite number of modes and to design a sensing system using lumped parameter approach. "Truncating" the model may lead to performance trade-off when designing a control system for distributed parameter systems. Lumped parameter approach is generally acceptable for sensing applications due to its nature of simplicity and ease of implementation. Although significant progress has been made in the recent past in the development of smart materials and structures featuring piezo-electric materials (Bailey and Hubbard, 1985; Plump et.al, 1987, Crawley, 19887), shape memory alloys (Miwn, 1985; Yaeger, 1984; Rogers and Robertshaw, 1988), electro-rheological fluids (Gandhi et al, 1989; Choi et al, 1989; Gandhi et al, 1989), and optical fibers (Morikawa, 1985; Rogowski, 1988), very few work have been done to characterize the dynamic behaviors of these devices, especially when it is used for high-speed applications.

Emphasis is placed on the accurate modeling and characterization of structural parameters of sensing devices for flexible structures. The analysis of a beam attached to a rotating base is a subject of interest to many researchers because numerous structural configurations such as spinning satellites (Laurenson, 1976; Kane et al., 1987) and flexible robots (Cannon and Schmitz, 1984; Mitchell and Bruch, 1988; Yang and Donath, 1988) fall into this category. The analysis of these rotating dynamic structures with payloads is quite different from those of stationary structures due to the inertia of gyroscopic effect at high rotating speeds.

Piezoelectric materials are media which develop mechanical strain when subjected to an electrical field, or conversely, they develop an electrical field when subjected to mechanical deformation. Their inherent high power-to-weight ratio makes them ideal candidates for embedding piezoelectric materials in traditional structures for vibration sensing and control. Crawley and de Luis (1987) studied the effect of a beam with bonded piezoelectric sensors. Plump et al. (1987) used a piezoelectric film to enhance the damping ratio of a cantilever beam. Tzou applied a piezoelectric film as an active vibration in a flexible structure (1987) and an active vibration isolator and exciter (1989). This paper focuses on the development of analytical models for dynamic characterization of a high-speed rotating flexible beam-mass system with embedded sensing system. The design of such a sensing system featuring piezoelectric materials is addressed. Several simulation examples are presented to validate the analytical solutions.

DESIGN AND ANALYSIS

Basic Assumptions and Coordinate Systems

To derive a simple yet effective sensing model for the physical system of interest, several assumptions are imposed here, namely:

(1) Large Overall Rigid-Body Displacements with Small Elastic Deformations: This assumption is valid for a mechanical system rotating at speeds less than one thousand revolutions per minute with low payload.

(2) Negligible Gravity Effect: For high-speed rotating space structure, the gravity effect can be ignored.

(3) Negligible Geometric Stiffening Effect: When rotating in plane, the magnitude of the axial displacement is much smaller than that of the transverse displacement. The effect of geometric stiffening is negligible.

(4) Plane Stress Condition: Since the beam is thin, the stress variation through the thickness is negligible.

(5) Average Material Properties: The average material properties of smart beams is used. Since the piezoelectric film is relatively thin, the isotropic aluminum beam plays a dominant role in contributing to the overall beam deflection. For structural monitoring, this assumption is valid.

$$\rho_{eq} = \frac{\rho_1 A_1 + \rho_2 A_2}{A}$$

$$E_{eq} = \frac{E_1 I_1 + E_2 I_2}{I} \qquad (1)$$

where A_1 is the cross sectional area of AL layer, A_2 is the cross sectional area of PVF_2 layer, I_1 is the moment of inertia of Aluminum layer about z axis, $I_1=b_1h_1^3/12$, and I_2 is the moment of inertia of PVF_2 layer about z axis, $I_2=b_2h_2^3/12$. The Euler-Bernoulli beam theory is used for dynamic formulation.

Two coordinate systems, one being the global X-Y and the other local x-y, are introduced to describe the dynamic system. The local coordinate system moves with the rigid body configuration of the link. Figures 1 and 2 show the schematic of the deflected

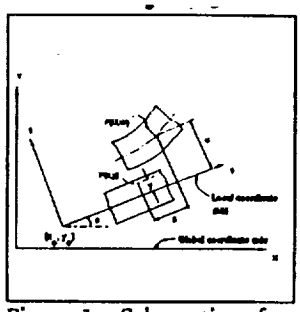

Figure 1: Schematic of a deflected beam element in local and global coordinate axes.

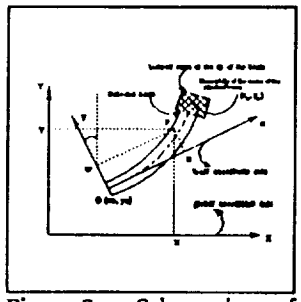

Figure 2: Schematic of rotating beam-mass system showing local and global coordinate axes

beam in both local and global coordinates. In classical small deflection beam theory, the displacements of an arbitrary point P(U, W) on a beam can be expressed in terms of homogenous coordinates as

$$\begin{Bmatrix} W \\ U \\ 1 \end{Bmatrix} = \begin{bmatrix} 1 & 0 & 0 & y \\ 0 & -y & 1 & x \\ 0 & 0 & 0 & 1 \end{bmatrix} \begin{Bmatrix} w \\ w' \\ u \\ 1 \end{Bmatrix} = B\{g\} \tag{2}$$

where x and y are the local coordinates of point P in the undeformed state. U and W are the local coordinates of point P after deformation. u, w, and w' are the axial, transverse and tangential displacements of point P, respectively. {g} is the displacement vector of point P in homogenous coordinates. The displacement vector, {g}, can be expressed in terms of nodal displacement vector {p} as $\{g\} = N\{p\}$, where $\{p\} = [\{q\}^T \mid 1]^T$, $\{q\} = [w_i\ w_i'\ u_i\ w_j\ w_j'\ u_j]^T$, and N, the shape function matrix, is given as

$$N = \begin{bmatrix} N_1 & N_2 & 0 & N_3 & N_4 & 0 & 0 \\ N_1' & N_2' & 0 & N_3' & N_4' & 0 & 0 \\ 0 & 0 & N_5 & 0 & 0 & N_6 & 0 \\ 0 & 0 & 0 & 0 & 0 & 0 & 1 \end{bmatrix} \tag{3}$$

where the shape functions, N_1, N_2, N_3, N_4, are the Hermite polynomials used for a beam element. N_5 and N_6 are the shape functions for a bar element in axial loading [24]. Note that $N_i' = dN_i/dx$. These shape functions are reported as

$$N_1 = 1-3(\frac{x}{L})^2+2(\frac{x}{L})^3; \quad N_2 = x(\frac{x}{L}-1)^2; \quad N_3 = (\frac{x}{L})^2(3-2\frac{x}{L})$$
$$N_4 = \frac{x^2}{L}(\frac{x}{L}-1); \quad N_5 = \frac{(L-x)}{L}; \quad N_6 = (\frac{x}{L}) \tag{4}$$

Substitute the expression of {g} into equation (2) to get

$$[W\ \ U\ \ 1]^T = B\,N\,\{p\} \tag{5}$$

and describe point P in terms of the global coordinates as

$$[X\ \ Y\ \ 1]^T = R\,B\,N\,\{p\} \tag{6}$$

where R is the transformation matrix that relates the local and global coordinate systems.

The expression for R is

$$R = \begin{bmatrix} -\sin\theta & \cos\theta & x_o \\ \cos\theta & \sin\theta & y_o \\ 0 & 0 & 1 \end{bmatrix} \tag{7}$$

where (x_0, y_0) are the coordinates of the origin of the local coordinate axis and θ is the angle between the local and global coordinate axes.

Elemental Equation of Motion

The variational principle (Washizu, 1968) for a dynamic system and the Lagrange equation are used to derive the element matrices. The first step in the finite element formulation is to discretize the domain of interest. The Lagrangian of a system is the sum of the Lagrangian of its constituting elements. In terms of the kinetic and potential energy, the Lagrange equation can be presented as

$$\begin{aligned} \sum_e Q_{(q)} &= \sum_e \left[\frac{d}{dt}\left(\frac{\partial T_e}{\partial \{\dot{q}\}}\right) - \frac{\partial T_e}{\partial \{q\}} + \frac{\partial U_e}{\partial \{q\}} \right] \\ &= \sum_e \left[\frac{d}{dt}\left(\frac{\partial T_b + T_m}{\partial \{\dot{q}\}}\right) - \frac{\partial T_b + T_m}{\partial \{q\}} + \frac{\partial U_e}{\partial \{q\}} \right] \\ &= \sum_e \left[(M_{2b} + M_{2m})\ddot{q} + (M_{1b} + M_{1m})\dot{q} + (M_{0b} + M_{0m})q + K_b q \right] \end{aligned} \tag{8}$$

where T_e and U_e are the kinetic and potential energy of a beam element. Note, that for the element connected to the payload block, $T_e = T_b + T_m$, T_b and T_m being the kinetic energies of the rotating beam and the tip mass attached at the end, respectively. U is the potential energy of the beam element, $\{q\}$ and $\{Q_q\}$ are the generalized coordinates and forces, respectively. The expressions of M_{2b}, M_{1b}, M_{0b}, K_b, M_{2m}, M_{1m}, M_{0m}, and Q are given below. The detailed derivation of these matrices are reported in Lai et al. (1992).

$$M_{2b} = \rho \begin{bmatrix} \frac{13}{35}AL + \frac{6I}{5L} & \frac{11}{210}AL^2 + \frac{I}{10} & 0 & \frac{9}{70}AL - \frac{6I}{5L} & -\frac{13}{420}AL^2 + \frac{I}{10} & 0 \\ & \frac{AL^3}{105} + \frac{2}{15}mL & 0 & \frac{13}{420}AL^2 - \frac{I}{10} & -\frac{AL^3}{140} - \frac{mL}{30} & 0 \\ & & \frac{AL}{3} & 0 & 0 & \frac{AL}{6} \\ & \text{symmetric} & & \frac{13}{35}AL + \frac{6I}{5L} & -\frac{11}{210}AL^2 - \frac{I}{10} & 0 \\ & & & & \frac{AL^3}{105} + \frac{2}{15}mL & 0 \\ & & & & & \frac{AL}{3} \end{bmatrix} \tag{9}$$

$$M_{1b} = \rho AL \begin{bmatrix} 0 & 0 & \frac{7}{10} & 0 & 0 & \frac{3}{10} \\ & 0 & \frac{L}{10} & 0 & 0 & \frac{L}{15} \\ & & 0 & -\frac{3}{10} & \frac{L}{15} & 0 \\ & \text{antisymmetric} & & 0 & 0 & \frac{7}{10} \\ & & & & 0 & -\frac{L}{10} \\ & & & & & 0 \end{bmatrix} \tag{10}$$

$$M_{0b} = \rho \begin{bmatrix} -(\frac{13AL}{35} + \frac{6I}{5L})\dot{\theta}^2 & -(\frac{11AL^2}{210} + \frac{I}{10})\dot{\theta}^2 & \frac{7AL}{20}\ddot{\theta} & (-\frac{9AL}{70} + \frac{6I}{5L})\dot{\theta}^2 & (\frac{13AL^2}{420} - \frac{I}{10})\dot{\theta}^2 & \frac{3AL}{20}\ddot{\theta} \\ -(\frac{11AL^2}{210} + \frac{I}{10})\dot{\theta}^2 & -(\frac{AL^3}{105} + \frac{2mL}{15})\dot{\theta}^2 & \frac{AL^2}{20}\ddot{\theta} & (-\frac{13AL^2}{420} + \frac{I}{10})\dot{\theta}^2 & (\frac{AL^3}{140} + \frac{mL}{30})\dot{\theta}^2 & \frac{AL^2}{30}\ddot{\theta} \\ -\frac{7AL}{20}\ddot{\theta} & -\frac{AL^2}{20}\ddot{\theta} & -\frac{AL}{3}\dot{\theta}^2 & (-\frac{3AL}{20})\ddot{\theta} & \frac{AL^2}{30}\ddot{\theta} & -\frac{AL}{6}\dot{\theta}^2 \\ (-\frac{9AL}{70} + \frac{6I}{5L})\dot{\theta}^2 & (-\frac{13AL^2}{420} + \frac{I}{10})\dot{\theta}^2 & (\frac{3AL}{20})\ddot{\theta} & -(\frac{13AL}{35} + \frac{6I}{5L})\dot{\theta}^2 & (\frac{11AL^2}{210} + \frac{I}{10})\dot{\theta}^2 & \frac{7AL}{20}\ddot{\theta} \\ (\frac{13AL^2}{420} - \frac{I}{10})\dot{\theta}^2 & (\frac{AL^3}{140} + \frac{mL}{30})\dot{\theta}^2 & -\frac{AL^2}{30}\ddot{\theta} & (\frac{11AL^2}{210} + \frac{I}{10})\dot{\theta}^2 & -(\frac{AL^3}{105} + \frac{2mL}{15})\dot{\theta}^2 & (-\frac{AL^2}{20})\ddot{\theta} \\ -\frac{3AL}{20}\ddot{\theta} & -\frac{AL^2}{30}\ddot{\theta} & -\frac{AL}{6}\dot{\theta}^2 & -\frac{7AL}{20}\ddot{\theta} & (\frac{AL^2}{20})\ddot{\theta} & -\frac{AL}{3}\dot{\theta}^2 \end{bmatrix} \tag{11}$$

$$M_{0b} = -\dot{\theta}^2 M_{2b} + \frac{\ddot{\theta}}{2} M_{1b} \tag{12}$$

$$Q_{1b} = \rho \begin{bmatrix} \frac{AL}{2}[y_c\cos(\theta) - z_c\sin(\theta)] - [I + \frac{3AL^2}{20}]\dot{\theta} \\ \frac{AL^2}{12}[y_c\cos(\theta) - z_c\sin(\theta)] + \frac{AL^2}{30}\ddot{\theta} \\ \frac{AL}{2}[y_c\sin(\theta) + z_c\cos(\theta)] - \frac{AL^2}{6}\dot{\theta}^2 \\ \frac{AL}{2}[y_c\cos(\theta) - z_c\sin(\theta)] - [I + \frac{7AL^2}{20}]\dot{\theta} \\ \frac{AL^2}{12}[-y_c\cos(\theta) + z_c\sin(\theta)] - \frac{AL^2}{20}\ddot{\theta} \\ \frac{AL}{2}[y_c\sin(\theta) + z_c\cos(\theta)] - \frac{AL^2}{3}\dot{\theta}^2 \end{bmatrix} \tag{13}$$

$$K_b = \begin{bmatrix} \frac{12EI}{L^3} & \frac{6EI}{L^2} & 0 & \frac{-12EI}{L^3} & \frac{6EI}{L^2} & 0 \\ & \frac{4EI}{L} & 0 & \frac{-6EI}{L^2} & \frac{2EI}{L} & 0 \\ & & \frac{EA}{L} & 0 & 0 & -\frac{EA}{L} \\ & \text{symmetric} & & \frac{12EI}{L^3} & \frac{-6EI}{L^2} & 0 \\ & & & & \frac{4EI}{L} & 0 \\ & & & & & \frac{EA}{L} \end{bmatrix} \tag{14}$$

where I and A represent the moment of inertia and the cross section area of the beam, respectively. The nonzero terms of M_{2m}, M_{1m}, M_{0m} and Q_{1m} matrices are given as

$$\begin{aligned}
&[M_{2m}]_{4,4} = M_m[1 - (y_c\sin w' - x_c\cos w')] \\
&[M_{2m}]_{5,5} = M_m[(c+1)(x_c^2+y_c^2) - (y_c+x_c)\sin w' - (y_c-x_c)\cos w'] \\
&[M_{2m}]_{6,6} = M_m[1 - (y_c\cos w' + x_c\sin w')] \\
&[M_{1m}]_{4,4} = 2M_m\dot{\theta}[(y_c\cos w' + x_c\sin w') - 1] \\
&[M_{1m}]_{5,5} = M_m(\dot{\theta} + \dot{w})[(y_c - x_c)\sin w' - (y_c + x_c)\cos w'] \\
&[M_{1m}]_{6,6} = 2M_m\dot{\theta}[1 - (y_c\sin w' - x_c\cos w')] \\
&[M_{0m}]_{4,4} = -M_m\dot{\theta}^2[1 - (y_c\sin w' - x_c\cos w')] - M_m\ddot{\theta}[1 - (y_c\cos w' + x_c\sin w')] \\
&[M_{0m}]_{4,6} = M_m\ddot{\theta}[1 - (y_c\sin w' - x_c\cos w')] - M_m\dot{\theta}^2[1 - (y_c\cos w' + x_c\sin w')] \\
&[Q_{1m}]_{4,1} = M_m\dot{\theta}[L - (y_c\sin w' - x_c\cos w')] - M_m\dot{\theta}^2(y_c\cos w' + x_c\sin w') \\
&[Q_{1m}]_{5,1} = M_m\ddot{\theta}[(x_c^2+y_c^2)(c+1) - L(y_c\sin w' - x_c\cos w')] + M_m\dot{\theta}^2L(y_c\cos w' + x_c\sin w') \\
&[Q_{1m}]_{6,1} = -M_m\ddot{\theta}(y_c\cos w' + x_c\sin w') - M_m\dot{\theta}^2[L - (y_c\sin w' - x_c\cos w')]
\end{aligned} \tag{15}$$

Note that the system mass matrix is the sum of the mass matrices of the tip mass and the beam element, i.e., $M_2 = M_{2b} + M_{2m}$, and so on.

System Equations and FEM Solution

The system governing equation is obtained in a two-stage procedure. In the first stage, the elemental equations of motion are generated. In the second stage, the elemental equations are assembled into a system equation. The detailed assembly procedure was presented by Fallahi and Lai (1992). The displacement is obtained by the integration of the system equation. The secondary information, such as the strain, stress, and induced electric voltage, are calculated using the result of finite element solutions.

Stress-Strain Relationship

The longitudinal strain ϵ_x is given as

$$\epsilon_x = \frac{\partial U}{\partial x} = u' - yw'' = [0 \;\; -y \;\; 1 \;\; 0] \begin{bmatrix} 0 & 0 & 0 & 0 & 0 & 0 & 0 \\ (-\frac{6}{L^2}+\frac{12x}{L^3}) & (\frac{4x}{L^2}-\frac{4}{L}) & 0 & (\frac{6}{L^2}-\frac{12x}{L^3}) & (\frac{6x}{L^2}-\frac{2}{L}) & 0 & 0 \\ 0 & 0 & -\frac{1}{L} & 0 & 0 & \frac{1}{L} & 0 \\ 0 & 0 & 0 & 0 & 0 & 0 & 0 \end{bmatrix} \begin{bmatrix} w_1 \\ w_1' \\ u_1 \\ w_2 \\ w_2' \\ u_2 \\ 1 \end{bmatrix} \tag{16}$$

C-2

Stress at the same point can be obtained by using

$$\sigma_x = E\,\epsilon_x \tag{17}$$

Dynamic Monitoring System

From these equations, strain and stress at any arbitrary point, p(x, y), on the beam element are computed. The voltage, V(x,t), generated by the piezo strain is calculated by

$$V(x,t) = e_p(x,t).(h_2/d_{31}) \tag{18}$$

where E is the modulus of elasticity, h is the thickness of the layers, V is the strain induced voltage, h_2 is the thickness of the PVF_2 layer, and d_{31} is the appropriate piezoelectric constant, and

$$e_p(x) = -\frac{E_1h_1 + E_2h_2}{E_2h_2}\,e_f(x) \tag{19}$$

The sensor configuration used in this study is a layer of PVF_2, polyvinylidene fluoride, bonded to one side of the rotating beam. Fig. 3 shows the cross sectional view of the beam with PVF_2 layer. PVF_2 is a polymer that can be polarized or made piezo-electrically active through appropriate processing during manufacture (Bailey and Hubbard, 1985). In its nonpolarized form, PVF_2 is a common electrical insulator. In it's polarized form PVF_2 is essentially a tough, flexible piezoelectric crystal. Polarized PVF_2 is commercially available as thin polymeric film having a layer of nickel or aluminum deposited on each face to conduct a voltage or applied across its faces in y-direction which results in a longitudinal strain in x-direction. This is the d_{31} component of the piezoelectric activity. If PVF_2 is polarized biaxially that would strain in both the x and the z directions. For this study we consider uniaxial PVF_2 only.

Fig. 4 shows the smart beam configuration. The longitudinal strain, ϵ_f, is obtained by force equilibrium in axial direction by finite element formulation. The strain, ϵ_p, in the PVF_2 layer introduce a corresponding piezo voltage to the PVF_2. The combined dynamic effect of gyroscopic, coriolis and other inertia are recorded by the piezo voltage. This voltage can be used as an monitoring index. When the index value exceeds the imposed constraints or material's natural constraints, the control action, i.e. the direct piezoelectric effect, can be triggered to take place.

Control Algorithm

The piezoelectric strain creates the net force in each layer acting as the moment arm from the midplane of the layer to the neutral axis of the beam, producing a bending moment

$$T(x,t) = E_1h_1b\epsilon_f\,[(h_1/2)-D] + E_2h_2b(\epsilon_p+\epsilon_f)\,[(h_2/2)+h_1-D] \tag{20}$$

where b is the width of the beam, and D is the location of the neutral axis of the composite beam given by

$$D = \frac{E_1h_1^2 + E_2h_2^2 + 2h_1h_2E_2}{2(E_1h_1+E_2h_2)} \tag{21}$$

Performing some algebraic manipulations to yield

$$T(x,t) = -V(x,t).d_{31}\left(\frac{h_1+h_2}{2}\right)\frac{E_1h_1E_2b}{(E_1h_1+E_2h_2)} - V(x,t).c \tag{22}$$

where c is constant for a given beam material and geometry expressing the bending moment per volt. If the material property and geometry of the composite beam change along its length, c is a function of x.

Combining the above equation with a conventional Euler-Bernoulli beam yields the equations of motion for transverse vibrations, w(x,t), of the composite beam. The governing equation becomes

$$\frac{\partial^2}{\partial x^2}[EI\frac{\partial^2 w}{\partial x^2} - c.V(x,t)] + \rho A\frac{\partial^2 w}{\partial t^2} = 0; \qquad for\ 0<x<L \tag{23}$$

and the boundary conditions are

$$\begin{aligned} w|_0 &= \frac{\partial w}{\partial x}|_0 = 0 \\ EI\frac{\partial^2 w}{\partial x^2}|_L &= -I_t\frac{\partial^3 w}{\partial t^2 \partial x}|_L + c.V(x,t) \\ EI\frac{\partial^3 w}{\partial x^3}|_L &= M_t\frac{\partial^2 w}{\partial x^2}|_L + c.\frac{\partial V(x,t)}{\partial x} \end{aligned} \tag{24}$$

where $EI = E_1I_1 + E_2I_2$, I is the area moment of inertia of the layer about the z axis, $\rho A = \rho A_1 + \rho A_2$, ρ is the density of the layer, A is the cross sectional area of the layer, and M_t and I_t the tip mass and tip inertia.

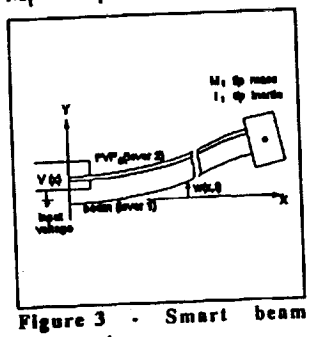

Figure 3 - Smart beam configuration

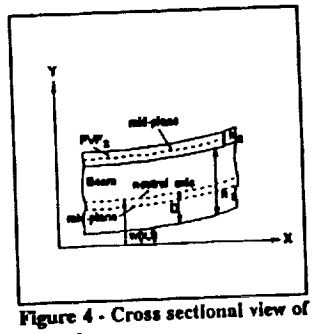

Figure 4 - Cross sectional view of smart beam

Since our PVF_2 has uniform geometry and a spatially uniform voltage applied along its length, the derivatives for the input voltage of the system becomes zero. The voltage that appears in the boundary condition can be used to control the bending moment. The functional of the system is formed by the squares of the curvature and the velocity as

$$J(w) = \frac{1}{2}\int_0^L [(\frac{\partial^2 w}{\partial t^2} + (\frac{\partial w}{\partial t})^2]dx \tag{25}$$

Applying the first variational principle we obtain the Euler-Lagrangian equation of motion, and both the essential and natural boundary conditions. Carrying out integration by parts of the first variation of the functional gives

$$\frac{\partial J}{\partial t} = \int_0^L (1-\frac{EI}{\rho A}).\frac{\partial^3 w}{\partial t \partial x^2}.\frac{\partial^2 w}{\partial x^2}dx - \frac{M_t}{\rho A}.\frac{\partial^2 w}{\partial t^2}.\frac{\partial w}{\partial t}|_L - \frac{I_t}{\rho A}.\frac{\partial^3 w}{\partial t^2 \partial x}.\frac{\partial^2 w}{\partial t \partial x}|_L + \frac{cV(t)}{\rho A}.\frac{\partial^2 w}{\partial t \partial x}|_L \tag{26}$$

The voltage appears only in one term. To extremize the functional, the voltage is chosen such that it appears as negative as

$$V = -sgn(c.\frac{\partial^2 w}{\partial x \partial t}|_L).V_{max} \tag{27}$$

where $\frac{\partial^2 w}{\partial t \partial x}|_L$ is the angular velocity at the tip of the beam. The control voltage is chosen to generate a bending moment that opposes the angular motion at the tip of the beam. The geometry of the piezoelectric layer can be tailored to obtain the necessary control function.

NUMERICAL EXPERIMENTS

Several numerical simulations are conducted to illustrate the effectiveness of the full beam formulation of the beam-mass system. A beam-mass system made of rectangular aluminum materials with an embedded PVF_2 layer is used for the study. The dimensions and material properties of the beam are given in Table 1. The beam is subjected to a spin-up maneuver (Kane, 1985) prescribed by

$$\theta = \begin{cases} \frac{\dot{\theta}_0}{T}[\frac{t^2}{2} + (\frac{T}{2\pi})^2(\cos\frac{2\pi t}{T} - 1)] ; & 0 \le t \le T \\ \dot{\theta}_0[t - \frac{T}{2}] ; & t > T \end{cases} \tag{29}$$

where $\dot{\theta}_0$ is the steady state angular velocity. In order to characterize the dynamic behavior of the system at different rotating speeds, we set the steady state speeds to 300, 500 and 700 rpm, and time constant, T, is 1 seconds. The simulation is carried out for a period of 5 seconds.

Table 1 - Geometric parameters and material properties of the smart beam

	Aluminum	PVF_2	Composite Beam
Length (L)	20	20	20
Thickness (h; in)	.9989	.0011	1
Width (w; in)	.25	.25	.25
Density (ρ; lb s^2/in^4)	2.45×10^{-4}	1.68×10^{-4}	2.45×10^{-4}
Young's Modulus (E; psi)	1×10^7	2.9×10^5	1×10^7
Static Piezo-electric Constant (d_{31};in/V)		8.66×10^{-10}	

Figures 5 and 6 show the transverse displacement, w, of the piezo-aluminum beam-mass system rotating at three different speeds. The transverse tip displacement of the beam is computed and recorded for both formulation with and without payload mass inertia. Both of the maximum transient tip displacement and the steady-state tip deflection are proportional to the size of the mass attachment. The contribution of gyroscopic terms is computed and recorded in Table 2. A maximum 4.35% contribution of gyroscopic inertia is observed at a speed of 700 rpm. The contribution becomes significant when the mass attachment is increased. The contribution of gyroscopic inertia becomes more pronounced when the speed is increased.

When 10% of a equivalent beam mass is attached to the tip of the rotating beam, the tip strain is increased at least two times. Figures 7 and 8 show the longitudinal tip strain at three different speeds. The corresponding longitudinal stresses are presented in Figures 9 and 10. These plots are similar to those of Figures 7 and 8 with an amplification in magnitude by the factor of an equivalent modulus of elasticity. The tip strain induced voltage of the piezoelectric layer at three speeds are presented in Figures 11 and 12. It is observed that the piezo voltage introduced by tip strain of no payload is in the range of 50 to 170 volts. The piezo voltage induced by the tip strain with a 10% tip mass attachment is in the range of 120 to 530 volts. The contribution of tip masses and speeds are

experimented to allow control voltage to be adjusted to the design range. The geometric parameters of both aluminum beams and piezoelectric layers are design variables to be tailored to satisfy the design need.

Table 2 - Contribution of gyroscopic terms at different speeds (*)

	Tip Mass Attached to Beam	Angular Velocity		
		300 rpm	500 rpm	700 rpm
Aluminum beam-mass system	0%	0.52%	1.02%	2.08%
	10%	0.67%	1.47%	3.20%
Piezo-aluminum beam-mass system	0%	0.69%	1.36%	2.80%
	10%	0.90%	2.08%	4.35%

(*) Percentage difference in steady-state solution at different speeds for M_0 and M_1

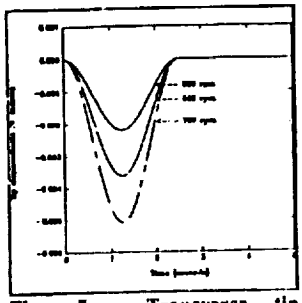

Figure 5 - Transverse tip displacements, w, of piezo-aluminum beam rotating at 300, 500 and 700 rpm

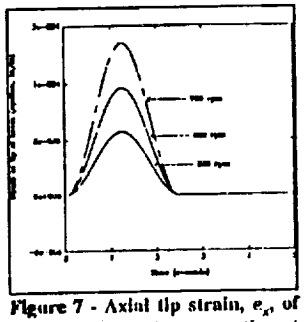

Figure 7 - Axial tip strain, e_x, of piezo-aluminum beam rotating at 300, 500, and 700 rpm

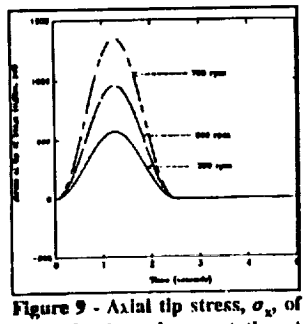

Figure 9 - Axial tip stress, σ_x, of piezo-aluminum beam rotating at speeds of 300, 500, and 700 rpm

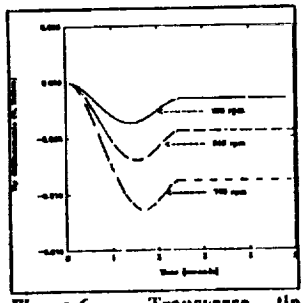

Figure 6 - Transverse tip displacements, w, of the piezo-aluminum beam-mass(10%) system rotating at 300, 500, and 700 rpm

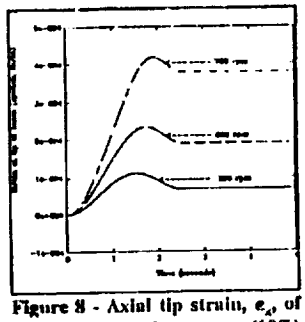

Figure 8 - Axial tip strain, e_x, of piezo-aluminumbeam-mass(10%) system rotating at 300, 500, and 700 rpm

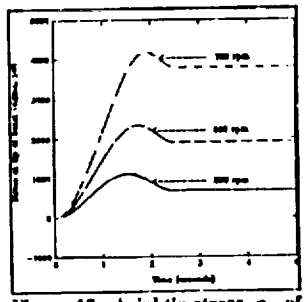

Figure 10 - Axial tip stress, σ_x, of piezo-aluminumbeam-mass(10%) system rotating at 300, 500, and 700 rpm

CONCLUSION

A systematic finite element based design method is presented in the paper. The method allows the a high-speed rotating dynamic structure with embedded piezoelectric films to be designed and monitored. The gyroscopic effect introduced by different payload at various speeds can be taken into consideration in the early design. The result of numerical simulations indicates that current approach can be used for application in the sensing and monitoring of high-speed spinning space structures and flexible mechanical systems. The finite element based method is simple and systematic. The dynamic characteristics of high speed rotating structures and machinery can be observed and used in distributed parameter models for control of such systems.

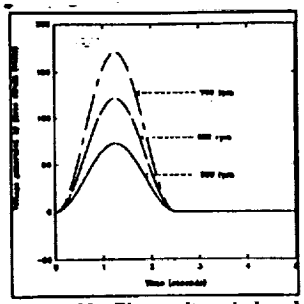

Figure 11 - Piezo voltage induced by the tip strain of piezo-aluminum beam rotating at 300, 500, and 700 rpm

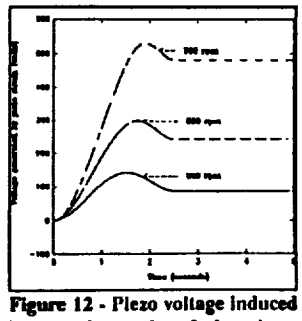

Figure 12 - Piezo voltage induced by the tip strain of the piezo-aluminum beam-mass (10%) system rotating at 300, 500, and 700 rpm

ACKNOWLEDGEMENT

The authors gratefully acknowledge the support provided by the United States Army Strategic Defense Command and the NASA Center for Aerospace Research at A&T.

REFERENCES

Bailey, T. and Hubbard Jr., J.E., 1985, Distributed Piezo-electric-Polymer Active Vibration Control of A Cantilever Beam, Journal of Guidance, Control and Dynamics, Vol. 8, No. 5, pp. 605-611, 1985.

Choi, S.B., Gandhi, M.V., and Thompson, B.S., 1989, An Active Vibration Tuning for Smart Flexible Structures Incorporating Electro-Rheological Fluids: A Proof-of-Concept Investigation, Proceedings of 1989 American Control Conference.

Crawley, E.F. and deLuis, J., 1987, Use of Piezoelectric Actuators as Elements of Intelligent Structures, AIAA Journal, Vol. 25, No. 10, pp. 1373-1385.

Fallahi, B., Lai, H.Y. and C. Venkat, 1992, A Comparative Study of the Finite Element Assembly Procedures Using Conventional and Modified Lagrange Equations, Canadian Society of Mechanical Engineering Forum 92.

Gandhi, M.V. and Thompson, B.S., 1989, Smart Materials and Structures Technologies: The Impending Revolution, Technomic Publishing Company, Inc., Lancaster, PA.

Gandhi, M.V., Thompson, B.S., and Choi, S.B., 1989, A New Generation of Innovative Ultra-Advanced Intelligent Composite Materials Featuring Electro-rheological Fluids: An Experimental Investigation, Journal of Composite Materials.

Gandhi, M.V., Thompson, B.S., Choi, S.B. and Shakir, S., 1989, Electro-Rheological-Fluid-Based Articulating Robotics Systems, ASME Journal of Mechanisms, Transmissions and Automation in Design.

Kane, T.R., Ryan, R.R., Banerjee, A.K., 1985, Dynamics of a Beam Attached to a Moving Base, AAS/AIAA Astrodynamics Specialist Conference, Paper AAS 85-390, Vail, Colorado.

Lai, H.Y., Fallahi, B. and R. Gupta, 1992, Full Beam Formulation of a Rotating Laminated Beam-Mass System, to appear in Composite Journal, Paper No. COMP/91/1008KK.

Morikawa, T., 1985, Optical Actuators, Japanese Journal of Society Instrumentation and Control Engineering, Vol. 24, No. 9, pp. 827-831.

Miwa, Y., 1985, Shape Memory Alloys Application for Sequential Operation Control, System and Control (Japan), Vol. 29, No. 5, pp. 303-310, 1985.

Plump, J.M., Hubbard Jr., J.E. and Bailey, T., 1987, Nonlinear Control of A Distributed System: Simulation and Experimental Results, ASME Journal of Dynamics, Measurement, and Control, Vol. 109, pp. 133-139.

Rogers, C.A. and Robertshaw, H.H., 1988, Shape Memory Alloy Reinforced Composites, Engineering Science Reprint 25, ESP25.88027, Society of Engineering Sciences Inc..

Rogowski, R.S., Heyman, J.S., and Claus, R.O., 1988, The Evolution of Smart Composite Materials, NASA Tech Briefs, Vol. 12, No. 10, pp. 20-22.

Tzou, H.S. and Tseng, C.I., 1990, Distributed Modal Identification and Vibration Control of Continua, Journal of Sound and Vibration, Vol. 138, No. 1, pp. 17-34.

Yaeger, J.R., 1984, A Practical Shape-Memory Electro-mechanical Actuator, ISATA 84 Proceedings, International Symposium on Automotive Technology and Automation, Milan, Italy, Vol. 1, pp. 633-642.